

# Sliding Mode Control of Fuel Cell, Supercapacitors and Batteries Hybrid Sources for Vehicle Applications

M. Y. Ayad<sup>1</sup>, M. Becherif<sup>2</sup>, A. Aboubou<sup>3</sup> and A. Henni<sup>4</sup>

<sup>1</sup>Industrial Hybrid Vehicle Applications,

<sup>2</sup>FEMTO-FC-Labs, UTBM University,

<sup>3</sup>LMSE Laboratory, Biskra University,

<sup>4</sup>UTBM University,

<sup>1, 2, 4</sup>France

<sup>3</sup>Algeria

## 1. Introduction

Fuel Cells (FC) produce electrical energy from an electrochemical reaction between a hydrogen-rich fuel gas and an oxidant (air or oxygen) (Kishinevsky & Zelingher, 2003) (Larminie & Dicks, 2000). They are high-current, and low-voltage sources. Their use in embedded systems becomes more interesting when using storage energy elements, like batteries, with high specific energy, and supercapacitors (SC), with high specific power. In embedded systems, the permanent source which can either be FC's or batteries must produce the limited permanent energy to ensure the system autonomy (Pischinger et al., 2006) (Moore et al., 2006) (Corrêa et al., 2003). In the transient phase, the storage devices produce the lacking power (to compensate for deficit in power required) in acceleration function, and absorbs excess power in braking function. FC's, and due to its auxiliaries, have a large time constant (several seconds) to respond to an increase or decrease in power output. The SCs are sized for the peak load requirements and are used for short duration load levelling events such as fuel starting, acceleration and braking (Rufer et al, 2004) (Thounthong et al., 2007). These short durations, events are experienced thousands of times throughout the life of the hybrid source, require relatively little energy but substantial power (Granovskii et al., 2006) (Benziger et al., 2006).

Three operating modes are defined in order to manage energy exchanges between the different power sources. In the first mode, the main source supplies energy to the storage device. In the second mode, the primary and secondary sources are required to supply energy to the load. In the third, the load supplies energy to the storage device.

We present in this work two hybrids DC power sources using SC as auxiliary storage device, a Proton Exchange Membrane-FC (PEMFC) as main energy source (Ayad et al., 2010) (Becherif et al., 2010) (Thounthong et al., 2007) (Rufer et al., 2004). The difference between the two structures is that the second contains a battery DC link. A single phase DC machine is connected to the DC bus and used as load. The general structures of the studied systems are presented and a dynamic model of the overall system is given in a state space

model. The control of the whole system is based on nonlinear sliding mode control for the DC-DC SCs converter and a linear regulation for the FC converter. Finally, simulation results using Matlab are given.

## 2. State of the art and potential application

### 2.1 Fuel cells

#### A. Principle

The developments leading to an operational FC can be traced back to the early 1800's with Sir William Grove recognized as the discoverer in 1839.

A FC is an energy conversion device that converts the chemical energy of a fuel directly into electricity. Energy is released whenever a fuel (hydrogen) reacts chemically with the oxygen of air. The reaction occurs electrochemically and the energy is released as a combination of low-voltage DC electrical energy and heat.

Types of FCs differ principally by the type of electrolyte they utilize (Fig. 1). The type of electrolyte, which is a substance that conducts ions, determines the operating temperature, which varies widely between types.

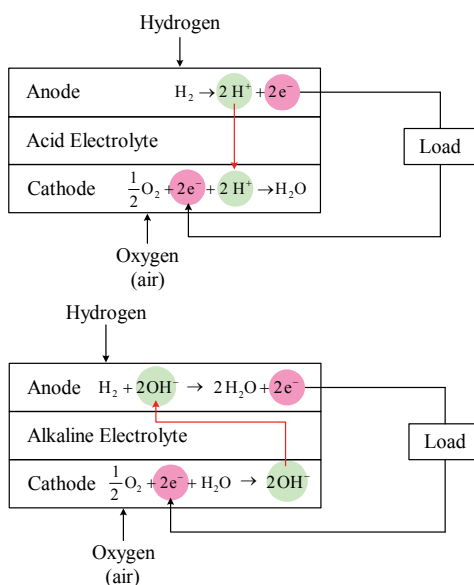


Fig. 1. Principle of acid (top) and alkaline (bottom) electrolyte fuel cells

Proton Exchange Membrane (or "solid polymer") Fuel Cells (PEMFCs) are presently the most promising type of FCs for automotive use and have been used in the majority of prototypes built to date.

The structure of a cell is represented in Fig. 2. The gases flowing along the x direction come from channels designed in the bipolar plates (thickness 1-10 mm). Vapour water is added to the gases to humidify the membrane. The diffusion layers (100-500  $\mu\text{m}$ ) ensure a good distribution of the gases to the reaction layers (5-50  $\mu\text{m}$ ). These layers constitute the

electrodes of the cell made of platinum particles, which play the role of catalyst, deposited within a carbon support on the membrane.

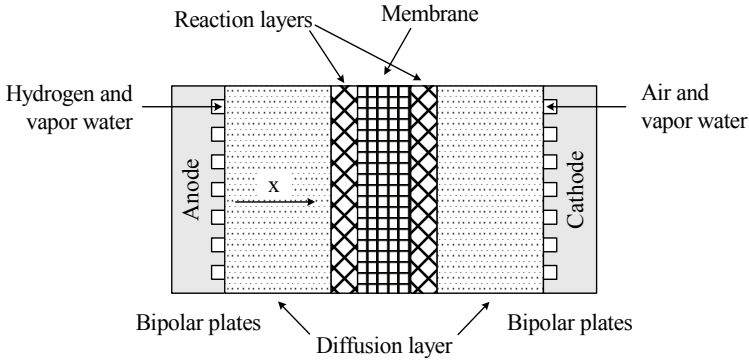
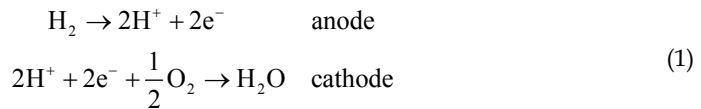


Fig. 2. Different layers of an elementary cell

Hydrogen oxidation and oxygen reduction:



The two electrodes are separated by the membrane (20-200 μm) which carries protons from the anode to the cathode and is impermeable to electrons. This flow of protons drags water molecules as a gradient of humidity leads to the diffusion of water according to the local humidity of the membrane. Water molecules can then go in both directions inside the membrane according to the side where the gases are humidified and to the current density which is directly linked to the proton flow through the membrane and to the water produced on the cathode side.

Electrons which appear on the anode side cannot cross the membrane and are used in the external circuit before returning to the cathode. Proton flow is directly linked to the current density:

$$J_{\text{H}^+} = \frac{i}{F}
 \tag{2}$$

where F is the Faraday's constant.

The value of the output voltage of the cell is given by Gibb's free energy ΔG and is:

$$V_{\text{rev}} = -\frac{\Delta G}{2.F}
 \tag{3}$$

This theoretical value is never reached, even at no load condition. For the rated current (around 0.5 A.cm<sup>-2</sup>), the voltage of an elementary cell is about 0.6-0.7 V.

As the gases are supplied in excess to ensure a good operating of the cell, the non-consumed gases have to leave the FC, carrying with them the produced water.

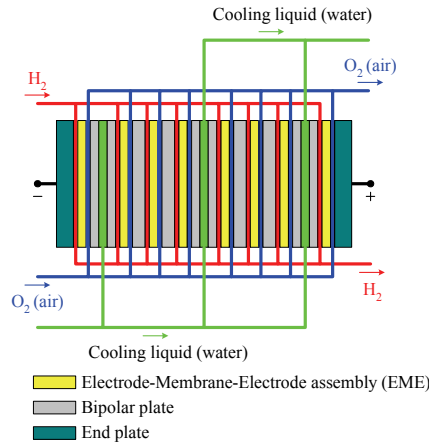


Fig. 3. External and internal connections of a PEMFC stack

Generally, a water circuit is used to impose the operating temperature of the FC (around 60-70 °C). At start up, the FC is warmed and later cooled as at the rated current nearly the same amount of energy is produced under heat form than under electrical form.

**B. Modeling Fuel Cell**

The output voltage of a single cell  $V_{FC}$  can be defined as the result of the following static and nonlinear expression (Larminie & Dicks, 2000):

$$V_{FC} = E - V_{act} - V_{ohm} - V_{concent} \tag{4}$$

where  $E$  is the thermodynamic potential of the cell and it represents its reversible voltage,  $V_{act}$  is the voltage drop due to the activation of the anode and of the cathode,  $V_{ohm}$  is the ohmic voltage drop, a measure of the ohmic voltage drop associated with the conduction of the protons through the solid electrolyte and electrons through the internal electronic resistances, and  $V_{concent}$  represents the voltage drop resulting from the concentration or mass transportation of the reacting gases.

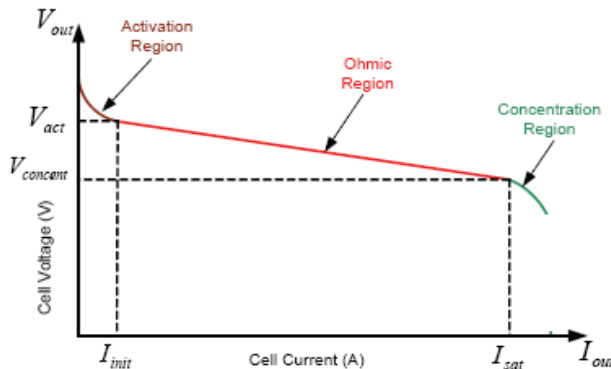


Fig. 4. A typical polarization curve for a PEMFC

In (4), the first term represents the FC open circuit voltage, while the three last terms represent reductions in this voltage to supply the useful voltage of the cell  $V_{FC}$ , for a certain operating condition. Each one of the terms can be calculated by the following equations,

$$\begin{aligned} V_{act} &= A \log\left(\frac{i_{FC} - i_n}{i_0}\right) \\ V_{ohm} &= R_m (i_{FC} - i_n) \\ V_{concent} &= b \log\left(1 - \frac{i_{FC} - i_n}{i_{lim}}\right) \end{aligned} \quad (5)$$

Hence,  $i_{FC}$  is the delivered current,  $i_0$  is the exchange current,  $A$  is the slope of the Tafel line,  $i_{Lim}$  is the limiting current,  $B$  is the constant in the mass transfer,  $i_n$  is the internal current and  $R_m$  is the membrane and contact resistances.

## 2.2 Electric double-layer supercapacitors

### A. Principle

The basic principle of electric double-layer capacitors lies in capacitive properties of the interface between a solid electronic conductor and a liquid ionic conductor. These properties discovered by Helmholtz in 1853 lead to the possibility to store energy at solid/liquid interface. This effect is called electric double-layer, and its thickness is limited to some nanometers (Belhachemi et al., 2000).

Energy storage is of electrostatic origin, and not of electrochemical origin as in the case of accumulators. So, supercapacitors are therefore capacities, for most of marketed devices. This gives them a potentially high specific power, which is typically only one order of magnitude lower than that of classical electrolytic capacitors.

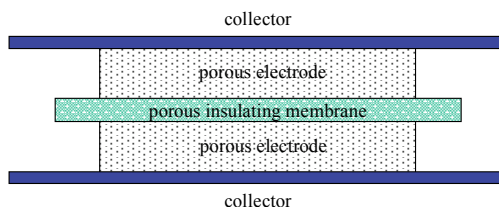


Fig. 5. Principle of assembly of the supercapacitors

In SCs, the dielectric function is performed by the electric double-layer, which is constituted of solvent molecules. They are different from the classical electrolytic capacitors mainly because they have a high surface capacitance ( $10\text{-}30 \mu\text{F}\cdot\text{cm}^{-2}$ ) and a low rated voltage limited by solvent decomposition (2.5 V for organic solvent). Therefore, to take advantage of electric double-layer potentialities, it is necessary to increase the contact surface area between electrode and electrolyte, without increasing the total volume of the whole.

The most widespread technology is based on activated carbons to obtain porous electrodes with high specific surface areas ( $1000\text{-}3000 \text{m}^2\cdot\text{g}^{-1}$ ). This allows obtaining several hundred of farads by using an elementary cell.

SCs are then constituted, as schematically presented below in Fig. 5, of:

- two porous carbon electrodes impregnated with electrolyte,
- a porous insulating membrane, ensuring electronic insulation and ionic conduction between electrodes,
- metallic collectors, usually in aluminium.

### B. Modeling and sizing of supercapacitors

Many applications require that capacitors be connected together, in series and/or parallel combinations, to form a “bank” with a specific voltage and capacitance rating. The most critical parameter for all capacitors is voltage rating. So they must be protected from over voltage conditions. The realities of manufacturing result in minor variations from cell to cell. Variations in capacitance and leakage current, both on initial manufacture and over the life of the product, affect the voltage distribution. Capacitance variations affect the voltage distribution during cycling, and voltage distribution during sustained operation at a fixed voltage is influenced by leakage current variations. For this reason, an active voltage balancing circuit is employed to regulate the cell voltage.

It is common to choose a specific voltage and thus calculating the required capacitance. In analyzing any application, one first needs to determine the following system variables affecting the choice of SC,

- the maximum voltage,  $V_{SCMAX}$
- the working (nominal) voltage,  $V_{SCNOM}$
- the minimum allowable voltage,  $V_{SCMIN}$
- the current requirement,  $I_{SC}$ , or the power requirement,  $P_{SC}$
- the time of discharge,  $t_d$
- the time constant
- the capacitance per cell,  $C_{SCcell}$
- the cell voltage,  $V_{SCcell}$
- the number of cell needs,  $n$

To predict the behavior of SC voltage and current during transient state, physics-based dynamic models (a very complex charge/discharge characteristic having multiple time constants) are needed to account for the time constant due to the double-layer effects in SC. The reduced order model for a SC cell is represented in Fig. 6. It is comprised of four ideal circuit elements: a capacitor  $C_{SCcell}$ , a series resistor  $R_S$  called the equivalent series resistance (ESR), a parallel resistor  $R_P$  and a series stray inductor  $L$  of  $\sim$ nH. The parallel resistor  $R_P$  models the leakage current found in all capacitors.

This leakage current varies starting from a few milliamps in a big SC under a constant current as shown in Fig. 7.

A constant discharging current is particularly useful when determining the parameters of the SC.

Nevertheless, Fig. 7 should not be used to consider sizing SCs for constant power applications, such as common power profile used in hybrid source.

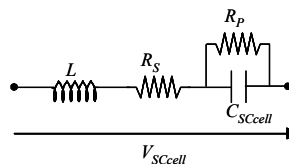


Fig. 6. Simple model of a supercapacitor cell

To estimate the minimum capacitance  $C_{SCMIN}$ , one can write an energy equation without losses ( $R_{ESR}$  neglected) as,

$$\frac{1}{2} C_{SCMIN} (V_{SCNOM}^2 - V_{SCMIN}^2) = P_{SC} t \tag{6}$$

with

$$P_{SC}(t) = V_{SC}(t) i_{SC}(t) \tag{7}$$

Then,

$$C_{SCMIN} = \frac{2P_{SC} t_d}{V_{SCNOM}^2 - V_{SCMIN}^2} \tag{8}$$

From (6) and (7), the instantaneous capacitor voltage and current are described as,

$$\begin{cases} V_{SC}(t) = V_{SCNOM} \sqrt{1 - \left(1 - \left(\frac{V_{SCNOM}}{V_{SCMIN}}\right)^2\right) \frac{t}{t_d}} \\ i_{SC}(t) = \frac{P_{SC}}{\sqrt{1 - \left(1 - \left(\frac{V_{SCNOM}}{V_{SCMIN}}\right)^2\right) \frac{t}{t_d}}} \end{cases} \tag{9}$$

Since the power being delivered is constant, the minimum voltage and maximum current can be determined based on the current conducting capabilities of the SC. (6) and (7) can then be rewritten as,

$$\begin{cases} V_{SCMIN} = \sqrt{V_{SCNOM}^2 - \frac{2P_{SC} t_d}{C_{MIN}}} \\ I_{SCMIN} = \frac{P_{SC}}{\sqrt{V_{SCNOM}^2 - \frac{2P_{SC} t_d}{C_{MIN}}}} \end{cases} \tag{10}$$

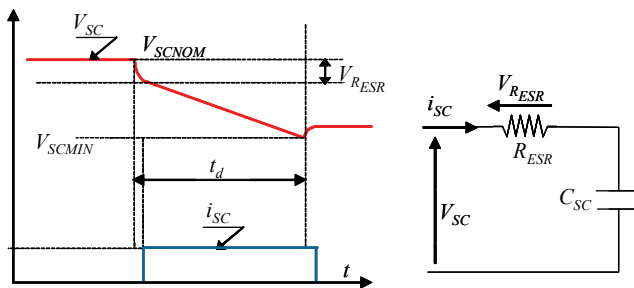


Fig. 7. Discharge profile for a SC under constant current.

The variables  $V_{SCMAX}$  and  $C_{SC}$  are indeed related by the number of cells  $n$ . The assumption is that the capacitors will never be charged above the combined maximum voltage rating of all the cells. Thus, we can introduce this relationship with the following equations,

$$\begin{cases} V_{SCMAX} = nV_{SCcell} \\ C_{SC} = \frac{C_{SCcell}}{n} \end{cases} \quad (11)$$

Generally,  $V_{SCMIN}$  is chosen as  $V_{SCMAX} / 2$ , from (6), resulting in 75% of the energy being utilized from the full-of-charge ( $SOC^1 = 100\%$ ). In applications where high currents are drawn, the effect of the  $R_{ESR}$  has to be taken into account. The energy dissipated  $W_{loss}$  in the  $R_{ESR}$ , as well as in the cabling, and connectors could result in an under-sizing of the number of capacitors required. For this reason, knowing SC current from (6), one can theoretically calculate these losses as,

$$W_{loss} = \int_0^{t_d} i_C^2(\tau) R_{ESR} d\tau = P_{SC} R_{ESR} C_{MIN} \ln\left(\frac{V_{SCNOM}}{V_{SCMIN}}\right) \quad (12)$$

To calculate the required capacitance  $C_{SC}$ , one can rewrite (6) as,

$$\frac{1}{2} C_{SCMIN} (V_{SCMAX}^2 - V_{SCMIN}^2) = P_{SC} t + W_{loss} \quad (13)$$

From (6) and (13), one obtains

$$\begin{cases} C_{SC} = C_{SCMIN} (1 + X) \\ X = \frac{W_{loss}}{P_{SC} t} \end{cases} \quad (14)$$

where  $X$  is the energy ratio.

From the equations above, an iterative method is needed in order to get the desired optimum value.

The differential capacitance can be represented by two capacitors: a constant capacitor  $C_0$  and a linear voltage dependent capacitor  $kV_0$ .  $k$  is a constant corresponding to the slope voltage. The SC is then modelled by:

$$\begin{cases} \frac{dV_0}{dt} = \frac{1}{C_0 + kV_0} i_{SC} \\ V_{SC} = R_{RSR} i_{SC} + V_0 \end{cases} \quad (15)$$

Where  $C_0 + kV_0 > 0$

### C. State of the art and potential application

Developed at the end of the seventies for signal applications (for memory back-up for example), SCs had at that time a capacitance of some farads and a specific energy of about  $0.5 \text{ Wh.kg}^{-1}$ .

---

<sup>1</sup> State Of Charge

High power SCs appear during the nineties and bring high power applications components with capacitance of thousand of farads and specific energy and power of several Wh.kg<sup>-1</sup> and kW.kg<sup>-1</sup>.

In the energy-power plan, electric double layers SCs are situated between accumulators and traditional capacitors.

Then these components can carry out two main functions:

- the function "source of energy", where SCs replace electrochemical accumulators, the main interest being an increase in reliability,
- the function "source of power", for which SCs come in complement with accumulators (or any other source limited in power), for a decrease in volume and weight of the whole system.

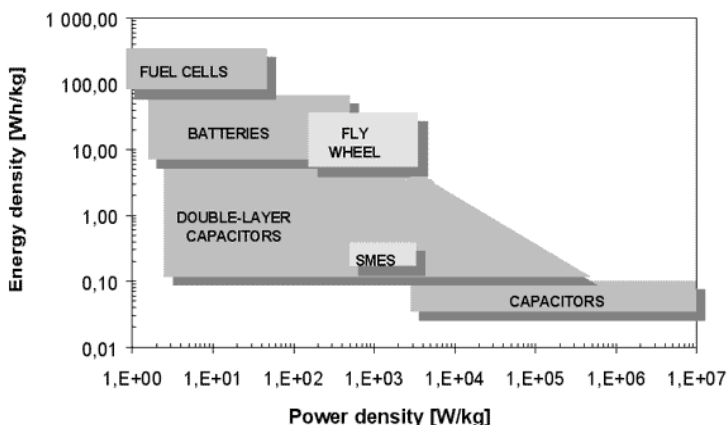


Fig. 8. Comparison between capacitors, supercapacitors, batteries and Fuel cell

### 2.3 State of the art of battery in electric vehicles

An electric vehicle (EV) is a vehicle that runs on electricity, unlike the conventional vehicles on road today which are major consumers of fossil fuels like gasoline. This electricity can be either produced outside the vehicle and stored in a battery or produced on board with the help of FC's.

The development of EV's started as early as 1830's when the first electric carriage was invented by Robert Andersen of Scotland, which appears to be appalling, as it even precedes the invention of the internal combustion engine (ICE) based on gasoline or diesel which is prevalent today. The development of EV's was discontinued as they were not very convenient and efficient to use as they were very heavy and took a long time to recharge.

This led to the development of gasoline based vehicles as the one pound of gasoline gave equal energy as a hundred pounds of batteries and it was relatively much easier to refuel and use gasoline. However, we today face a rapid depletion of fossil fuel and a major concern over the noxious green house gases their combustion releases into the atmosphere causing long term global crisis like climatic changes and global warming. These concerns are shifting the focus back to development of automotive vehicles which use alternative fuels for operations. The development of such vehicles has become imperative not only for the scientists but also for the governments around the globe as can be substantiated by the Kyoto Protocol which has a total of 183 countries ratifying it (As on January 2009).

### A. Batteries technologies

A battery is a device which converts chemical energy directly into electricity. It is an electrochemical galvanic cell or a combination of such cells which is capable of storing chemical energy. The first battery was invented by Alessandro Volta in the form of a voltaic pile in the 1800's. Batteries can be classified as primary batteries, which once used, cannot be recharged again, and secondary batteries, which can be subjected to repeated use as they are capable of recharging by providing external electric current. Secondary batteries are more desirable for the use in vehicles, and in particular traction batteries are most commonly used by EV manufacturers. Traction batteries include Lead Acid type, Nickel and Cadmium, Lithium ion/polymer, Sodium and Nickel Chloride, Nickel and Zinc.

	Lead Acid	Ni - Cd	Ni - MH	Li - Ion	Li - polymer	Na - NiCl <sub>2</sub>	Objectives
Specific Energy (Wh/Kg)	35 - 40	55	70 - 90	125	155	80	200
Specific Power (W/Kg)	80	120	200	260	315	145	400
Energy Density (Wh/m <sup>3</sup> )	25 - 35	90	90	200	165	130	300
Cycle Life (No. of charging cycles)	300	1000	600	+ 600	+ 600	600	1000

Table 1. Comparison between different batteries technologies.

The battery for electrical vehicles should ideally provide a high autonomy (i.e. the distance covered by the vehicle for one complete discharge of the battery starting from its potential) to the vehicle and have a high specific energy, specific power and energy density (i.e. light weight, compact and capable of storing and supplying high amounts of energy and power respectively). These batteries should also have a long life cycle (i.e. they should be able to discharge to as near as it can be to being empty and recharge to full potential as many number of times as possible) without showing any significant deterioration in the performance and should recharge in minimum possible time. They should be able to operate over a considerable range of temperature and should be safe to handle, recyclable with low costs. Some of the commonly used batteries and their properties are summarized in the Table 1.

### B. Principle

A battery consists of one or more voltaic cell, each voltaic cell consists of two half-cells which are connected in series by a conductive electrolyte containing anions (negatively charged ions) and cations (positively charged ions). Each half-cell includes the electrolyte and an electrode (anode or cathode). The electrode to which the anions migrate is called the anode and the electrode to which cations migrate is called the cathode. The electrolyte connecting these electrodes can be either a liquid or a solid allowing the mobility of ions.

In the redox reaction that powers the battery, reduction (addition of electrons) occurs to cations at the cathode, while oxidation (removal of electrons) occurs to anions at the anode. Many cells use two half-cells with different electrolytes. In that case each half-cell is enclosed in a container, and a separator that is porous to ions but not the bulk of the electrolytes prevents mixing. The figure 10 shows the structure of the structure of Lithium-Ion battery using a separator to differentiate between compartments of the same cell utilizing two respectively different electrolytes

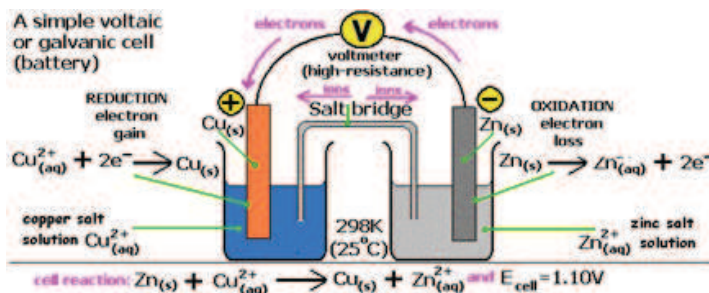


Fig. 9. Showing the apparatus and reactions for a simple galvanic Electrochemical Cell

### Structure of Lithium-Ion Battery

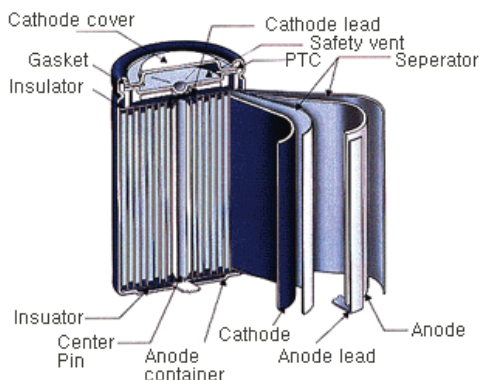


Fig. 10. Structure of Lithium-Ion Battery

Each half cell has an electromotive force (or emf), determined by its ability to drive electric current from the interior to the exterior of the cell. The net emf of the battery is the difference between the emfs of its half-cells. Thus, if the electrodes have emfs  $E_1$  and  $E_2$ , then the net emf is  $E_{\text{cell}} = E_2 - E_1$ . Therefore, the net emf is the difference between the reduction potentials of the half-cell reactions.

The electrical driving force or  $\Delta V_{\text{Bat}}$  across the terminals of a battery is known as the terminal voltage and is measured in volts. The terminal voltage of a battery that is neither charging nor discharging is called the open circuit voltage and equals the emf of the battery.

An ideal battery has negligible internal resistance, so it would maintain a constant terminal voltage until exhausted, then dropping to zero. If such a battery maintained 1.5 volts and stored a charge of one Coulomb then on complete discharge it would perform 1.5 Joule of work.

$$\text{Work done by battery (W)} = - \text{Charge} \times \text{Potential Difference} \quad (16)$$

$$\text{Charge} = \frac{\text{Coulomb}}{\text{Mole Electrons}} \times \text{Moles Electrons} \quad (17)$$

$$W = -nFE_{\text{cell}} \quad (18)$$

Where  $n$  is the number of moles of electrons taking part in redox,  $F = 96485$  coulomb/mole is the Faraday's constant i.e. the charge carried by one mole of electrons.

The open circuit voltage,  $E_{\text{cell}}$  can be assumed to be equal to the maximum voltage that can be maintained across the battery terminals. This leads us to equating this work done to the Gibb's free energy of the system (which is the maximum work that can be done by the system)

$$\Delta G = W_{\text{max}} = -nFE_{\text{cell}} \quad (19)$$

### C. Model of battery

Non Idealities in Batteries: Electrochemical batteries are of great importance in many electrical systems because the chemical energy stored inside them can be converted into electrical energy and delivered to electrical systems, whenever and wherever energy is needed. A battery cell is characterized by the open-circuit potential ( $V_{\text{OC}}$ ), i.e. the initial potential of a fully charged cell under no-load conditions, and the cut-off potential ( $V_{\text{cut}}$ ) at which the cell is considered discharged. The electrical current obtained from a cell results from electrochemical reactions occurring at the electrode-electrolyte interface. There are two important effects which make battery performance more sensitive to the discharge profile:

- Rate Capacity Effect: At zero current, the concentration of active species in the cell is uniform at the electrode-electrolyte interface. As the current density increases the concentration deviates from the concentration exhibited at zero current and state of charge as well as voltage decrease (Rao et al., 2005)
- Recovery Effect: If the cell is allowed to relax intermittently while discharging, the voltage gets replenished due to the diffusion of active species thereby giving it more life (Rao et al., 2005)

### D. Equivalent electrical circuit of battery

Many electrical equivalent circuits of battery are found in literature. (Chen et al., 2006) presents an overview of some much utilized circuits to model the steady and transient behavior of a battery. The Thevenin's circuit is one of the most basic circuits used to study the transient behavior of battery is shown in figure 11.

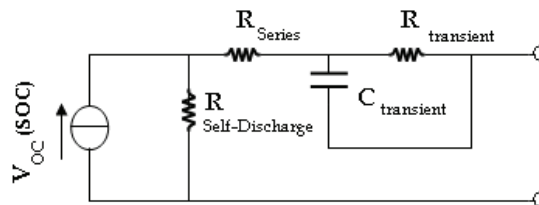


Fig. 11. Thevenin's model

It uses a series resistor ( $R_{series}$ ) and an RC parallel network ( $R_{transient}$  and  $C_{transient}$ ) to predict the response of the battery to transient load events at a particular state of charge by assuming a constant open circuit voltage [ $V_{oc}(SOC)$ ] is maintained. This assumption unfortunately does not help us analyze the steady-state as well as runtime variations in the battery voltage. The improvements in this model are done by adding more components in this circuit to predict the steady-state and runtime response. For example, (Salameh at al., 1992) uses a variable capacitor instead of  $V_{oc}$  (SOC) to represent nonlinear open circuit voltage and SOC, which complicates the capacitor parameter.

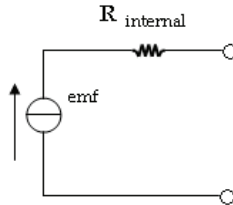


Fig. 12. Circuit showing battery emf and internal resistance  $R_{internal}$

However, in our study we are mainly concerned with the recharging of this battery which occurs while braking. The SC coupled with the battery accumulates high amount of charge when breaks are applied and this charge is then utilized to recharge the battery. Therefore, the design of the battery is kept to a simple linear model which takes into account the internal resistance ( $R_{internal}$ ) of the battery and assumes the emf to be constant throughout the process (Figure. 12).

### 3. Control of the hybrid sources based on FC, SCs and batteries

#### 3.1 Structures of the hybrid power sources

As shown in Fig. 13, the first hybrid source comprises a DC link supplied by a PEMFC and an irreversible DC-DC converter which maintains the DC voltage  $V_{DL}$  to its reference value, and a supercapacitive storage device, which is connected to the DC link through a current reversible DC-DC converter allowing recovering or supplying energy through SC.

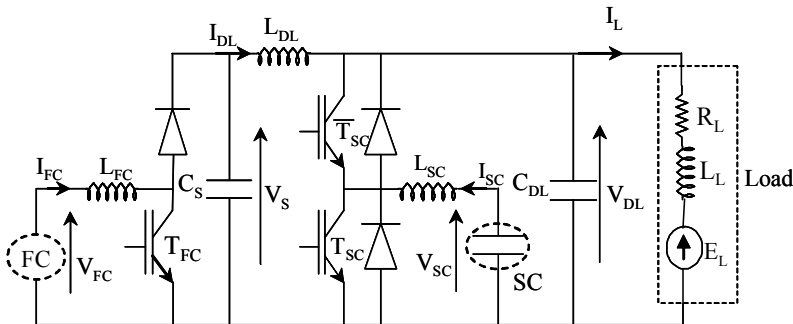


Fig. 13. Structure of the first hybrid source

The second system, shown in Fig. 14, comprises of a DC link directly supplied by batteries, a PEMFC connected to the DC link by means of boost converter, and a supercapacitive

storage device connected to the DC link through a reversible current DC-DC converter. The role of FC and the batteries is to supply mean power to the load, whereas the storage device is used as a power source: it manages load power peaks during acceleration and braking.

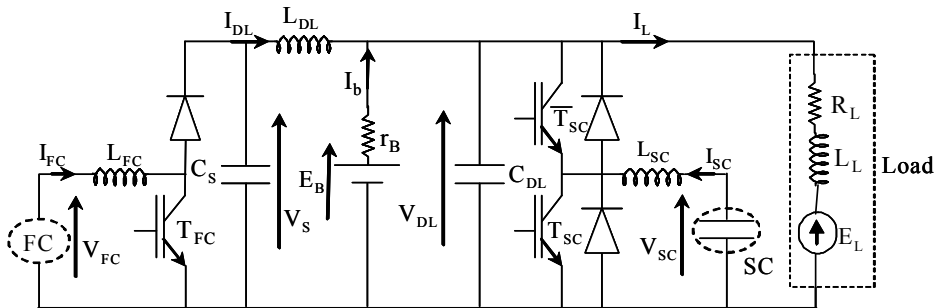


Fig. 14. Structure of the second hybrid source

### 3.2 Problem formulation

Both structures are supplying energy to the DC bus where a DC machine is connected. This machine plays the role of the load acting as a motor or as a generator when braking. The main purpose of the study is to present a control technique for the two hybrid source with two approaches. Two control strategies, based on sliding mode control have been considered, the first using a voltage controller and the second using a current controller. The second aim is to maintain a constant mean energy delivered by the FC, without a significant power peak, and the transient power is supplied by the SCs. A third purpose consists in recovering energy through the charge of the SC.

After system modeling, equilibrium points are calculated in order to ensure the desired behavior of the system. When steady state is reached, the load has to be supplied only by the FC source. So the controller has to maintain the DC bus voltage to a constant value and the SCs current has to be cancelled. During transient, the power delivered by the DC source has to be as constant as possible (without a significant power peak), and the transient power has to be delivered through the SCs. The SCs in turn, recover their energy during regenerative braking when the load provides current.

At equilibrium, the SC has to be charged and then the current has to be equal to zero.

### 3.3 Sliding mode control of the hybrid sources

Due to the weak request on the FC, a classical PI controller has been adapted for the boost converter. However, because of the fast response in the transient power and the possibility of working with a constant or variable frequency, a sliding mode control (Ayad et al., 2007), has been chosen for the DC-DC bidirectional SC converter. The bidirectional property allows the management of charge- discharge cycles of the SC tank.

The current supplied by the FC is limited to a range  $[I_{MIN}, I_{MAX}]$ . Within this interval, the FC boost converter ensures current regulation (with respect to reference). Outside this interval, i.e. when the desired current is above  $I_{MAX}$  or below  $I_{MIN}$ , the boost converter saturates and the surge current is then provided or absorbed by the storage device. Hence the DC link current is kept equal to its reference level. Thus, three modes can be defined to optimize the functioning of the hybrid source:

- *The normal mode*, for which load current is within the interval  $[I_{MIN}, I_{MAX}]$ . In this mode, the FC boost converter ensures the regulation of the DC link current, and the control of the bidirectional SC converter leads to the charge or the discharge of SC up to a reference voltage level  $V_{SCREF}$
- *The discharge mode*, for which load power is greater than  $I_{MAX}$ . The current reference of the boost is then saturated to  $I_{MAX}$ , and the FC DC-DC converter ensures the regulation of the DC link voltage by supplying the lacking current, through SC discharge,
- *The recovery mode*, for which load power is lower than  $I_{MIN}$ . The power reference of the FC boost converter is then saturated to  $I_{MIN}$ , and the FC DC-DC converter ensures the regulation of the DC link current by absorbing the excess current, through SC charge.

**A. DC-DC boost FC converter control principle**

Fig. 15 presents the synoptic control of the first hybrid FC boost. The FC current reference is generated by means of a PI voltage loop control on a DC link voltage and its reference:

$$I_{FC}^* = k_{PF1}(V_{DL}^* - V_{DL}) + k_{IF1} \int_0^t (V_{DL}^* - V_{DL}) dt \tag{20}$$

With,  $k_{PF1}$  and  $k_{IF1}$  are the proportional and integral gains.

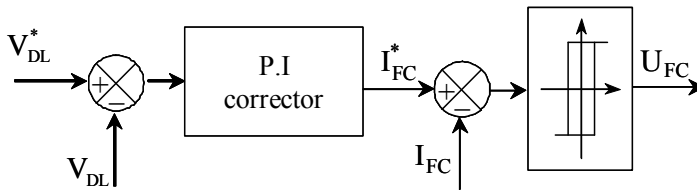


Fig. 15. Control of the FC converter

The second hybrid source FC current reference  $I_{FC}^*$  is generated by means of a PI current loop control on a DC link current and load current and the switching device is controller by a hysteresis comparator:

$$I_{FC}^* = k_{PF2}(I_L - I_{DL}) + k_{IF2} \int_0^t (I_L - I_{DL}) dt \tag{21}$$

With,  $k_{PF2}$  and  $k_{IF2}$  are the proportional and integral gains.

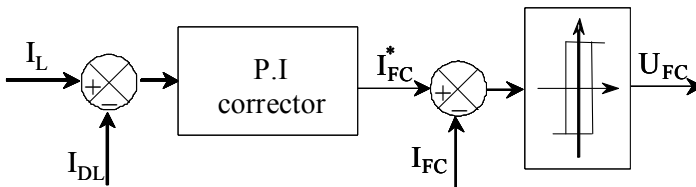


Fig. 16. Control of the FC converter

The switching device is controlled by a hysteresis comparator.

## B. DC-DC Supercapacitors converter control principle

To ensure proper functioning for the three modes, we have used a sliding mode control strategy for the DC-DC converter. Here, we define a sliding surface  $S_1$ , for the first hybrid source, as a function of the DC link voltage  $V_{DL}$ , its reference  $V_{DL}^*$ , the SCs voltage  $V_{SC}$ , its reference  $V_{SC}^*$ , and the SCs current  $I_{SC}$ :

$$S_1 = k_{11}(V_{DL} - V_{DL}^*) + k_{21} \cdot (I_{SC} - I_1) \quad (22)$$

with

$$I = k_{ps1}(V_{SC} - V_{SC}^*) + k_{is1} \int_0^t (V_{SC} - V_{SC}^*) dt \quad (23)$$

With,  $k_{ps1}$  and  $k_{is1}$  are the proportional and integral gains.

The FC PI controller ensures that  $V_{DL}$  tracks  $V_{DL}^*$ . The SC PI controller ensures that  $V_{SC}$  tracks its reference  $V_{SC}^*$ .

$k_{11}$ ,  $k_{21}$  are the coefficients of proportionality, which ensure that the sliding surface equal zero by tracking the SC currents to its reference  $I$  when the FC controller can't ensure that  $V_{DL}$  tracks  $V_{DL}^*$ .

In steady state condition, the FC converter ensures that the first term of the sliding surface is null, and the integral term of equation (23) implies  $V_{SC} = V_{SC}^*$ . Then, imposing  $S_1 = 0$  leads to  $I_{SC} = 0$ , as far as the boost converter output current  $I_{DL}$  is not limited. So that, the storage element supplies energy only during power transient and  $I_{DL}$  limitation.

For the second hybrid source, we define a sliding surface  $S_2$  as a function of the DC link current  $I_{DL}$ , The load current  $I_L$ , the SC voltage  $V_{SC}$ , its reference  $V_{SC}^*$ , and the SC current  $I_{SC}$ :

$$S_2 = k_{12}(I_{DL} - I_L) + k_{22}(I_{SC} - I_2) \quad (24)$$

with

$$I_2 = k_{ps2}(V_{SC} - V_{SC}^*) + k_{is2} \int_0^t (V_{SC} - V_{SC}^*) dt \quad (25)$$

With,  $k_{ps2}$  and  $k_{is2}$  are the proportional and integral gains.

The FC PI controller ensures that  $I_{DL}$  tracks  $I_L$ . The SC PI controller ensures that  $V_{SC}$  tracks its reference  $V_{SC}^*$ .

$k_{12}$ ,  $k_{22}$  are the coefficients of proportionality, which ensure that the sliding surface equal zero by tracking the SC currents to its reference  $I$  when the FC controller can't ensure that  $I_{DL}$  tracks  $I_L$ .

In the case of a variable frequency control, a hysteresis comparator is used with the sliding surface  $S$  as input. In the case of a constant frequency control, the general system equation can be written as:

$$\dot{X}_i = A_i X_i + B_i U_i + C_i + \xi_i \quad (26)$$

with  $i=1,2$

With for the first system:

$$X_1 = [V_{DL} \quad I_{SC} \quad V_{SC} \quad I]^T \tag{27}$$

and

$$A_1 = \begin{bmatrix} 0 & 1/C_{DL} & 0 & 0 \\ -1/L_{SC} & -r_{SC}/L_{SC} & 1/L_{SC} & 0 \\ 0 & -1/C_{SC} & 0 & 0 \\ 0 & -k_{ps1}/C_{SC} & k_{is1} & 0 \end{bmatrix}, B_1 = \begin{bmatrix} -I_{SC} & V_{DL} & 0 & 0 \\ C_{DL} & L_{SC} & 0 & 0 \end{bmatrix}^T,$$

$$U_1 = U_{SC}, \quad \xi_1 = [0 \quad 0 \quad 0 \quad 0]^T \text{ and } C_1 = \begin{bmatrix} (I_{DL} - I_L) & 0 & 0 & -k_{is} V_{SC}^* \\ C_{DL} & & & \end{bmatrix}^T$$

If we note:

$$G_1 = [k_{11} \quad k_{21} \quad 0 \quad -k_{21}] \tag{28}$$

the sliding surface is then given by:

$$S_1 = G_1 \cdot (X_1 - X_{ref1}) \tag{29}$$

with

$$X_{ref1} = [V_{DL}^* \quad 0 \quad 0 \quad 0]^T$$

With for the second system:

$$X_2 = [V_{DL} \quad I_{SC} \quad V_{SC} \quad I]^T$$

and

$$A_2 = \begin{bmatrix} -1/(r_B \cdot C_{DL}) & 1/C_{DL} & 0 & 0 \\ -1/L_{SC} & -r_{SC}/L_{SC} & 1/L_{SC} & 0 \\ 0 & -1/C_{SC} & 0 & 0 \\ 0 & -k_{ps2}/C_{SC} & k_{is2} & 0 \end{bmatrix}, B_2 = \begin{bmatrix} -I_{SC} & V_{DL} & 0 & 0 \\ C_{DL} & L_{SC} & 0 & 0 \end{bmatrix}^T,$$

$$\xi_2 = \begin{bmatrix} (I_{DL} - I_L) & 0 & 0 & 0 \\ C_{DL} & & & \end{bmatrix}^T, C_2 = \begin{bmatrix} E_B & 0 & 0 & -k_{is} V_{SC}^* \\ (r_B \cdot C_{DL}) & & & \end{bmatrix}^T, U_2 = U_{SC}$$

If we note:

$$G_2 = [k_{12} \quad k_{22} \quad 0 \quad -k_{22}] \tag{30}$$

the sliding surface is then given by:

$$S_2 = C_{DL} \xi_2 + G_2 X_2 \tag{31}$$

In order to set the system dynamic, we define the reaching law:

$$\dot{S}_i = -\lambda_i S_i - K_i \text{sign}(S_i) \tag{32}$$

with  $i=1,2$

$$K_i = 0 \quad \text{if } \|S_i\| < \varepsilon_i. \quad (33)$$

and

$$K_i = n_i \lambda_i \varepsilon_i \quad \text{if } \|S_i\| > \varepsilon_i. \quad (34)$$

The linear term  $-\lambda_i S_i(X)$  imposes the dynamic to remain inside the error bandwidth  $\varepsilon_i$ . The choice of a high value of  $\lambda_i$  ( $\leq f_c/2$ ) ensures a small static error when  $\|S_i\| < \varepsilon_i$ . The nonlinear term  $-K_i \cdot \text{sign}(S_i)$  permits to reject perturbation effects (uncertainty of the model, variations of the working conditions). This term allows compensating high values of error  $\|S_i\| > \varepsilon_i$  due to the above mentioned perturbations. The choice of a small value of  $\varepsilon_i$  leads to high current undulation (chattering effect) but the static error remains small. A high value of  $\varepsilon$  obliges to reduce the value of  $\lambda_i$  to ensure the stability of the system and leads to higher static error. Once the parameters ( $\lambda_i, K_i, \varepsilon_i$ ) of the reaching law are determined, it is possible to calculate the continuous equivalent control, which allows to maintain the state trajectory on the sliding surface. We use the equations (28), (27) and (29), we find for the first system:

$$U_{SC1} = (G_1 B_1)^{-1} \{-G_1 A_1 X_1 - G_1 C_1 + G_1 X_{ref1} - \lambda_1 G_1 X_1 + \lambda_1 G_1 X_{ref1} - K_1 \text{sign}(S_1)\} \quad (35)$$

Equations (26), (28) and (30) are used, we find for the second system:

$$U_{SC2} = (G_2 B_2)^{-1} \{-G_2 A_2 X_2 - G_2 C_2 - \lambda_2 G_2 X_2 - K_2 \text{sign}(S_2) - C_{DL} [\dot{\xi}_2 + \lambda_2 \xi_2]\} \quad (36)$$

The control laws (35) and (36) contain the attractive and the equivalent controls. These equations (35) and (36) give for both hybrid sources the equation:

$$A_{eqi} = A_i - B_i (G_i B_i)^{-1} G_i A_i - B_i (G_i B_i)^{-1} \lambda_i G_i \quad (37)$$

The equation (27) allows finding poles of the systems during the sliding motion as a function of  $\lambda_i, k_{1i}$  and  $k_{2i}$ . The parameters  $k_{isi}$  and  $k_{psi}$  are then determined by solving  $S_i=0$ , equation justified by the fact that the sliding surface dynamic is hugely much greater than SC voltage variation.

### C. Stability

Consider the following Lyapunov function:

$$V_i = \frac{1}{2} S_i^2 \quad (38)$$

With  $S$  is the sliding surface,  $i=1,2$ .

The derivative of the Lyapunov function along the trajectory of (15) is:

$$\dot{V}_i = S_i \dot{S}_i = -\lambda_i S_i^2 - K_i S_i \text{sign}(S_i) \leq 0 \quad (39)$$

With  $\lambda_i, K_i > 0$

Hence, the origin, with the sliding surface giving by (22) and (24), is globally asymptotically stable since the Lyapunov function (38) is radially unbounded and its derivative is strictly negative when  $S_i \neq 0$  and  $V_i = 0 \Leftrightarrow S_i = 0$ .

### 3.4 Simulation results of the hybrid sources control

The whole system has been implemented in the Matlab-Simulink Software with the following parameters associated to the hybrid sources:

- FC parameters:  $P_{FC} = 130 \text{ W}$ .
- DC link parameters:  $V_{DL} = 24 \text{ V}$ .
- SC parameters:  $C_{SC} = 3500/6 \text{ F}$ ,  $V_{SC}^* = 15 \text{ V}$ .

The results presented in this section have been carried out by connecting the hybrid source to a " $R_L, L_L$  and  $E_L$ " load representing a single phase DC machine.

Figures 17 and 18 present the behavior of currents  $I_{DL}$ ,  $I_L$ ,  $I_{SC}$ , and the DC link voltage  $V_{DL}$  for transient responses obtained while moving from the normal mode to the discharge mode, using sliding mode control. The test is performed by sharply changing the e.m.f load voltage  $E_L$  in the interval of  $t \in [1.5s, 5s]$ . The load current  $I_L$  changes from 16.8A to 24A. The current load  $I_L = 16.8\text{A}$  corresponds to a normal mode and the current load  $I_L = 24\text{A}$  to a discharge mode.

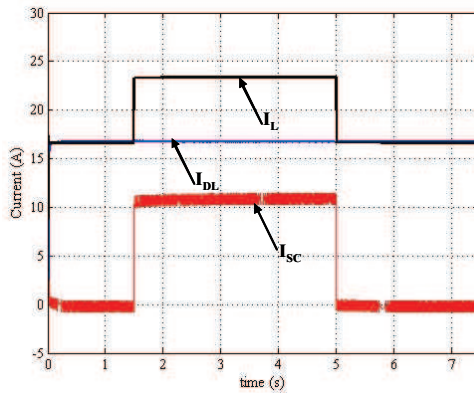


Fig. 17. FC, SCs and load currents

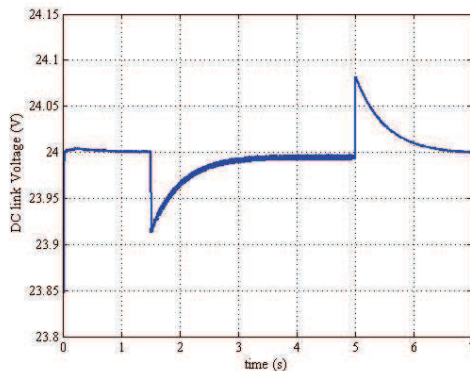


Fig. 18. DC link voltage

At the starting of the system, only FC provides the mean power to the load. The storage device current reference is equal to zero, when we are in normal mode. In the transient state, the load current  $I_L$  becomes lower than the DC link current  $I_{DL}$ . The DC link voltage

reference is set at 24V. The DC link voltage tracks the reference well during the first second, after which, a very small overshoot is observed when the load current becomes negative. Then, the storage device current reference becomes negative because the controller compensates the negative load current value by the difference between the SC voltage and its reference. This is the recovering mode. After the load variation ( $t > 5s$ ), the current in the DC link becomes equal to the load current. The SC current  $I_{SC}$  becomes null.

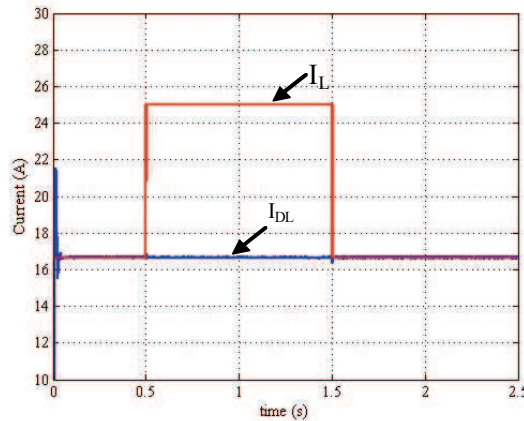


Fig. 19. Load and DC link currents

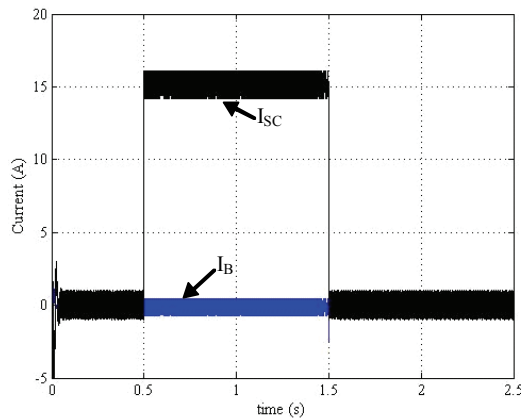


Fig. 20. SC and batteries currents

Figures 19, 20 and 21 present the behavior of currents  $I_{DL}$ ,  $I_L$ ,  $I_{SC}$ ,  $I_B$  and the DC link voltage  $V_{DL}$  for transient responses obtained for a transition from the normal mode to the discharge mode applying using sliding mode control. The test is performed by changing sharply the e.m.f load voltage  $E_L$  in the interval of  $t \in [0.5s, 1.5s]$ . The load current  $I_L$  changes from 16.8A to 25A. The current load  $I_L = 16.8A$  corresponds to a normal mode and the current load  $I_L = 25A$  to a discharge mode.

At the starting of the system, only the FC provides the mean power to the load. The storage device current reference is equal to zero, we are in normal mode. In the transient

state, the load current  $I_L$  became greater than the DC link current  $I_{DL}$ . The storage device current reference became positive thanks to control function which compensates this positive value by the difference between the SC voltage and its reference. We are in discharging mode. After the load variation ( $t > 1.5s$ ), the current in the DC link became equal to the load current. The SC current  $I_{SC}$  became null. We have a small variation in the batteries currents.

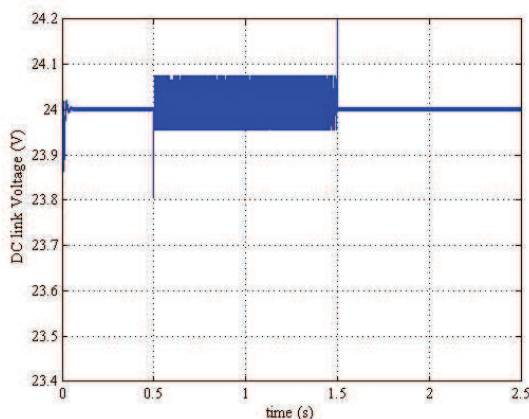


Fig. 21. DC link voltage

### 3. Conclusion

In this paper, the modeling and the control principles of two DC hybrid source systems have been presented. These systems are composed of a fuel cell source, SuperCapacitor source and with or without batteries on DC link. The state space models are given for both structures. These sources use the fuel cell as mean power source and supercapacitors as auxiliary transient power sources.

For the two hybrid structures, Sliding Mode Control principles have been applied in order to obtain a robustness control strategy. The sliding surface is generated as a function of multiple variables: DC link voltage and current, supercapacitors current and voltage, Load current.

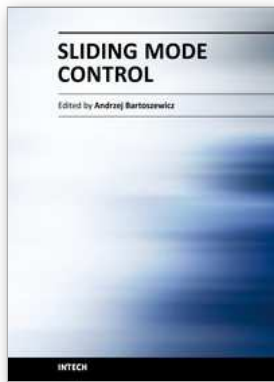
Global asymptotic stability proofs are given and encouraging simulation results has been obtained.

Many benefits can be expected from the proposed structures such as supplying and absorbing the power peaks by using supercapacitors which also allows recovering energy.

### 4. References

- Kishinevsky, Y. & Zelingher, S. (2003). Coming clean with fuel cells, IEEE Power & Energy Magazine, vol. 1, issue: 6, Nov.-Dec. 2003, pp. 20-25.
- Larminie, J. & Dicks, A. (2000). Fuel cell systems explained, Wiley, 2000.
- Pischinger, S.; Schönfelder, C. & Ogrzewalla, J. (2006). Analysis of dynamic requirements for fuel cell systems for vehicle applications, J. Power Sources, vol. 154, no. 2, pp. 420-427, March 2006.

- F. Belhachemi, S. Rael and B. Davat "A Physical based model of power electric double layer supercapacitors", IAS 2000, 35<sup>th</sup> IEEE Industry Applications Conference, Rome, 8-12 October
- Moore, R. M.; Hauer, K. H.; Ramaswamy, S. & Cunningham, J. M. (2006). Energy utilization and efficiency analysis for hydrogen fuel cell vehicles, *J. Power Sources*, 2006.
- Corbo, P.; Corcione, F. E.; Migliardini, F. & Veneri, O. (2006). Experimental assessment of energy-management strategies in fuel-cell propulsion systems, *J. Power Sources*, 2006.
- Rufer, A.; Hotellier, D. & Barrade, P. (2004). A Supercapacitor-Based Energy-Storage Substation for Voltage - Compensation in Weak Transportation Networks," *IEEE Trans. Power Delivery*, vol. 19, no. 2, April 2004, pp. 629-636.
- Thounthong, P.; Raël, S. & Davat, B. (2007). A new control strategy of fuel cell and supercapacitors association for distributed generation system, *IEEE Trans. Ind. Electron*, Volume 54, Issue 6, Dec. 2007 Page(s): 3225 - 3233
- Corrêa, J. M.; Farret, F. A.; Gomes, J. R. & Simões, M. G. (2003). Simulation of fuel-cell stacks using a computer-controlled power rectifier with the purposes of actual high-power injection applications, *IEEE Trans. Ind. App.*, vol. 39, no. 4, pp. 1136-1142, July/Aug. 2003.
- Benziger, J. B.; Satterfield, M. B.; Hogarth, W. H. J.; Nehlsen, J. P. & Kevrekidis; I. G. (2006). The power performance curve for engineering analysis of fuel cells, *J. Power Sources*, 2006.
- Granovskii, M.; Dincer, I. & Rosen, M. A. (2006). Environmental and economic aspects of hydrogen production and utilization in fuel cell vehicles, *J. Power Sources*, vol. 157, pp. 411-421, June 19, 2006
- Ayad, M. Y.; Pierfederici, S.; Raël, S. & Davat, B. (2007). Voltage Regulated Hybrid DC Source using supercapacitors, *Energy Conversion and Management*, Volume 48, Issue 7, July 2007, Pages 2196-2202.
- Rao, V.; Singhal, G.; Kumar, A. & Navet, N. (2005). Model for Embedded Systems Battery, *Proceedings of the 18th International Conference on VLSI Design held jointly with 4th International Conference on Embedded Systems Design (IEEE-VLSID'05)*, 2005.
- Chen, M.; Gabriel, A.; Rincon-Mora. (2006). Accurate Electrical Battery Model Capable of Predicting Runtime and  $I-V$  Performance. . *IEEE Trans. Energy Convers*, Vol. 21, No.2, pp.504-511 June 2006.
- Salameh, Z.M.; Casacca, M.A. & Lynch, W.A. (1992). A mathematical model for lead-acid batteries, *IEEE Trans. Energy Convers.*, vol. 7, no. 1, pp. 93-98, Mar. 1992.
- Jonathan J. Awerbuch and Charles R. Sullivan, "Control of Ultracapacitor-Battery Hybrid Power Source for Vehicular Applications", Atlanta, Georgia, USA 17-18 November 2008
- Ayad, M. Y.; Becherif, M.; Henni, A.; Wack, M. and Aboubou A. (2010). "Vehicle Hybridization with Fuel Cell, Supercapacitors and batteries by Sliding Mode Control", *Proceeding IEEE-ICREGA'10* – March 8<sup>th</sup>-10<sup>th</sup> Dubai
- Becherif, M.; Ayad, M. Y.; Henni, A.; Wack, M. and Aboubou A. (2010). "Control of Fuel Cell, Batteries and Solar Hybrid Power Source", *Proceeding IEEE-ICREGA'10*-- March 8<sup>th</sup>-10<sup>th</sup> Dubai
- M. Chen, A. Gabriel and Rincon-Mora, "Accurate Electrical Battery Model Capable of Predicting Runtime and  $I-V$  Performance", *IEEE Trans. Energy Convers*, Vol. 21, No.2, pp.504-511 June 2006.
- Z.M. Salameh, M.A. Casacca and W.A. Lynch, "A mathematical model for lead-acid batteries", *IEEE Trans. Energy Convers.*, vol. 7, no. 1, pp. 93-98, Mar. 1992.



## **Sliding Mode Control**

Edited by Prof. Andrzej Bartoszewicz

ISBN 978-953-307-162-6

Hard cover, 544 pages

**Publisher** InTech

**Published online** 11, April, 2011

**Published in print edition** April, 2011

The main objective of this monograph is to present a broad range of well worked out, recent application studies as well as theoretical contributions in the field of sliding mode control system analysis and design. The contributions presented here include new theoretical developments as well as successful applications of variable structure controllers primarily in the field of power electronics, electric drives and motion steering systems. They enrich the current state of the art, and motivate and encourage new ideas and solutions in the sliding mode control area.

### **How to reference**

In order to correctly reference this scholarly work, feel free to copy and paste the following:

M. Y. Ayad, M. Becherif, A. Aboubou and A. Henni (2011). Sliding Mode Control of Fuel Cell, Supercapacitors and Batteries Hybrid Sources for Vehicle Applications, Sliding Mode Control, Prof. Andrzej Bartoszewicz (Ed.), ISBN: 978-953-307-162-6, InTech, Available from: <http://www.intechopen.com/books/sliding-mode-control/sliding-mode-control-of-fuel-cell-supercapacitors-and-batteries-hybrid-sources-for-vehicle-applicati>

# **INTECH**

open science | open minds

### **InTech Europe**

University Campus STeP Ri  
Slavka Krautzeka 83/A  
51000 Rijeka, Croatia  
Phone: +385 (51) 770 447  
Fax: +385 (51) 686 166  
[www.intechopen.com](http://www.intechopen.com)

### **InTech China**

Unit 405, Office Block, Hotel Equatorial Shanghai  
No.65, Yan An Road (West), Shanghai, 200040, China  
中国上海市延安西路65号上海国际贵都大饭店办公楼405单元  
Phone: +86-21-62489820  
Fax: +86-21-62489821

© 2011 The Author(s). Licensee IntechOpen. This chapter is distributed under the terms of the [Creative Commons Attribution-NonCommercial-ShareAlike-3.0 License](#), which permits use, distribution and reproduction for non-commercial purposes, provided the original is properly cited and derivative works building on this content are distributed under the same license.